JOURNAL OF MATERIALS SCIENCE **39** (2004) 2801–2810

Characterization of optically active and photocurable ORMOSIL thin films deposited using the Aerosol process

M. TREJO-VALDEZ
LMGP/ENSPG, BP 46, Domaine Universitaire, 38402 Saint Martin d'Hères, France

P. JENOUVRIER
LMGP/ENSPG, BP 46, Domaine Universitaire, 38402 Saint Martin d'Hères, France; IMEP/ENSERG, UMR 5130, INPG-UJF-CNRS, BP 257, 38016 Grenoble, France

J. FICK
IMEP/ENSERG, UMR 5130, INPG-UJF-CNRS, BP 257, 38016 Grenoble, France

M. LANGLET*
LMGP/ENSPG, BP 46, Domaine Universitaire, 38402 Saint Martin d'Hères, France
E-mail: Michel.Langlet@inpg.fr

Aerosol-gel process is a deposition method based on the sol-gel polymerization of a liquid film produced from an ultrasonically sprayed aerosol. This process offers an attractive alternative for the deposition of photocurable SiO_2—TiO_2 ORMOSIL films. 3-(trimethoxysilyl) propylmethacrylate and tetraisopropyl-orthotitanate complexed with methacrylic acid were used as sol-gel precursors. Doping with a terbium:sulphosalicylic acid complex was also studied to test the deposition of spectroscopically active photocurable films. FTIR spectroscopy has been used to study the precursor solutions and ORMOSIL films. It is shown that titanium precursor incorporation enhances the solution reactivity, which yields optical quality thin films. Photopolymerization and photoluminescence properties of the films are reported and discussed with respect to the experimental parameters. The results allow envisaging the UV-imprinting fabrication of Aerosol-gel-derived active waveguides.

1. Introduction

Since pioneering works performed in the early 1980s [1, 2], the sol-gel preparation of organic-inorganic hybrid materials has attracted a continuously growing interest both from industrial and academic point of view [3]. These materials are also mentioned in the literature as ORMOSILs (organically modified silicates), ormocers® (organically modified ceramics), ceramers (ceramic polymers), or other denominations. For simplicity, in this paper we will use the "ORMOSIL" nomenclature. The main interest of ORMOSILs arises from their ability to combine the potentialities of inorganic and organic chemistry. New or enhanced properties induced by the organic component can therefore be obtained, which could not be possible using a traditional inorganic sol-gel route. For this reason, ORMOSILs have been extensively studied in numerous application fields including optics, electronics, ionics, mechanics, membranes, protective coatings, catalysis, sensors, and biology [3, 4]. Recently, photosensitive sol-gel ORMOSIL films composed of a mixed methacrylate/silicate network have been studied for planar optical waveguide applications, as a new alternative to traditional silica and polymer materials [5–14]. 3-(trimethoxysilyl) propylmethacrylate (MTPS) was used as a photopolymerizable component. Under UV-light irradiation, the acrylate function undergoes photopolymerization, which induces in turn densification of the ORMOSIL film. Thus, optical steps can be selectively UV-imprinted, which allows the fabrication of integrated optical devices.

Besides, ORMOSIL films elaborated at low temperature present a rather small content in OH groups, when compared to traditional sol-gel silica films elaborated at the same temperature. For this reason, ORMOSIL films have been proposed as host matrices of rare-earth ions for applications in integrated active optics [4]. A low OH content is an important feature to take into account for the fabrication of active waveguides, because photoluminescence (PL) quenching by OH groups, via multiphonon relaxation effects, severely limits the rare-earth spectroscopic efficiency [4]. Low temperature processing of rare-earth doped ORMOSIL films would allow the fabrication of integrated active devices on thermally

*Author to whom all correspondence should be addressed.

sensitive supports, such as polymers. However, even the weak OH content of ORMOSIL films remains a problem when considering a low temperature elaboration approach. An interesting way to overcome this problem is based on the rare-earth encapsulation into an organic cage, through complexation of the rare-earth precursor with a suitable organic compound [15, 16]. Due to encapsulation, rare-earth ions are efficiently protected against detrimental interactions with OH groups. Encapsulation is also expected to prevent short-range interactions between vicinal rare-earth ions, which could nearly totally quench the PL through concentration quenching mechanisms. Moreover, rare-earth encapsulation yields a significant enhancement of the overall PL efficiency based on indirect pumping, i.e, pumping of the strong UV-absorption band of the organic complex, followed by energy transfer to the rare-earth ion [15, 17].

Generally, sol-gel films are deposited using the traditional spin- and dip-coating techniques. Both methods involve batch deposition procedures. They are well adapted to the deposition of films on large but essentially planar supports. Besides, some works have been devoted to the development of new sol-gel deposition methods. Over the ten past years, an original deposition technique has been developed in our department, the Aerosol-gel process [18]. This technique is based on the sol-gel transformation of a liquid film deposited from an ultrasonically generated aerosol, which is conducted onto the substrate surface using a carrier gas. Owing to its principle, this technique is technologically very different from traditional spin- and dip-coating methods. The process implementation involves a continuous in-time deposition procedure, which allows a precise and flexible control of the film thickness through a simple adjustment of the deposition time. As it is a gaseous transport assisted method, it allows a careful separation of the liquid deposition and sol-gel transformation steps through a simple change of the deposition atmosphere, which favors a precise control of the experimental conditions. Finally, the system lends itself to the deposition on large and three-dimensional substrates and it is compatible with in-line technologies for high throughput mass production, which are normally used in CVD industrial deposition. The industrial potential of the Aerosol-gel process has been demonstrated in collaboration with various European companies. For instance, an in-line deposition prototype was constructed to coat "23 inch" (=584 mm) cathode ray tubes with thickness uniformity better than 2% [19]. Our recent works demonstrated the versatility of the Aerosol-gel process to deposit thin films of various compositions. In particular, rare earth doped vitreous silica [20–22] and nanocrystallized multicomponent transparent thin films [23, 24] were successfully deposited for applications in integrated active optics. Up to now, the Aerosol-gel deposition of ORMOSIL films had never been studied. The possibility to deposit such films would increase again the potential of this technique.

In this paper, we report the first attempts to deposit photocurable MTPS-derived ORMOSIL films using the Aerosol-gel process. In addition, ORMOSIL films elaborated at low temperature have been doped with terbium ions using the organic encapsulation approach. In a previous work, we showed that Aerosol-gel deposited SiO_2—TiO_2 films doped with a terbium:sulphosalicylic acid (SSA) complex exhibited a substantial spectroscopic activity after a heat-treatment at only 150°C [22]. The terbium:SSA encapsulation approach has been extrapolated to MTPS-derived ORMOSIL films. In this study, we focus on the feasibility of photocurable, optically active, and homogeneous films of good optical quality and controlled thickness. The solution preparation and film deposition conditions are described. Photopolymerization and PL properties of the films are discussed in relation to the experimental parameters.

2. Experimental

2.1. Solution and film preparation

Aerosol-gel precursor solutions were prepared from 3-(trimethoxysilyl) propylmethacrylate (MTPS), deionized water, absolute ethanol, hydrochloric acid (HCl), methacrylic acid (MAA), tetraisopropyl-orthotitanate (TIPT), terbium chloride, and sulphosalicylic acid (SSA). In some cases, benzildimethylketal (BZK: Irgacure 651 furnished by CIBA) was used as photoinitiator (3 wt% in the final solution). MTPS was used as matrix precursor. TIPT was used to tailor the film refractive index. Several Si:Ti molar ratios were tested in the 10:0 to 10:6 range. The solutions were prepared using a multi-step procedure. In a first step, pre-hydrolysis of MTPS was carried out by adding acidified water (0.2 M HCl) in a H_2O to MTPS molar ratio (r_w) of 0.6. At the same time, but in a separate flask, TIPT was complexed with methacrylic acid in TIPT:MAA molar ratios of 1:1 or 1:2. After 45 min, both solutions were mixed together under vigorous stirring. In a next step, additional water was incorporated ($r_w = 1.6$), in order to complete the hydrolysis reaction and to enhance the solution reactivity. Terbium chloride, complexed in ethanol with SSA using a previously published procedure [22], was finally added to the ORMOSIL solution. The SSA:Tb molar ratio was fixed at 0.5:1. The resulting solution was then diluted with various amount of absolute ethanol in order to study a [0.154–1.904 M] MTPS + TIPT concentration range. In this article, the concentration (C) will now refer to the MTPS + TIPT concentration. The pH of the solution varied from 2 to 3, depending on the dilution degree in ethanol. The Tb concentration in the final solution was fixed at 11.6×10^{-2} M, which corresponded to a Tb/Si + Ti molar ratio of 4 mol%.

Solutions were then tested for Aerosol-gel deposition of ORMOSIL films. Precursor solutions were stored in a glass vessel fitted with a piezoelectric transducer and fed with a constant level burette. The transducer was excited at its resonance frequency (around 800 kHz). An aerosol composed of microscopic droplets was produced at the liquid surface under the effects of ultrasonic excitation. Then, the so-formed aerosol was transported onto the substrate surface (silicon wafers or silica plates) using an air flux regulated with flowmeters. After reaching the substrate, the droplets underwent

surface spreading and coalescence. It has previously been shown that preventing a premature polycondensation reaction is a key factor that favors a total surface coalescence of the droplets and promotes the formation of homogeneous films [25]. For that purpose, the carrier gas was super-saturated with methanol-ethanol mixture using bubbling systems. Any premature polycondensation, which could be induced by solvent evaporation during droplet transport, was thus prevented. Methanol has been used to saturate the carrier gas together with ethanol because, as it is a MTPS hydrolysis product, it appears in significant amount within the final hydrolyzed solution. The whole deposition device was enclosed in a cabinet thermallized at 20°C. Plate supporting the substrate, pulverization vessel, and bubbling systems were also individually regulated at 20°C. After liquid film deposition, the dilution solvent was allowed to vaporize under dry air flux. In the same time, the liquid film reacted through the classic hydrolysis/polycondensation sol-gel route, resulting in a solid xerogel film. At this point, the xerogel film was recuperated and stored at ambient conditions, or heat-treated in air for 2 h at various temperatures up to 250°C, before characterization.

2.2. Solution and film characterization

Dynamic viscosity of the solutions was measured using a rotating cylinder viscosimeter (Rheovisco ELV-8). Fourier transform infrared (FTIR) spectroscopy has been used to identify chemical species present in the precursor solutions and ORMOSIL films, and to study photopolymerization features. FTIR spectra were acquired using a Bio-rad FTS-165 spectrometer. The precursor solutions were investigated by ATR (attenuated total reflection)-FTIR spectroscopy in the (4000–500 cm^{-1}) spectral range. For that purpose, small aliquots of the solutions were spread at the surface of a ZnSe prism and enclosed in a sealed cell to avoid any solvent evaporation and sol-gel reaction during spectrum acquisition. The Tb:SSA complex formed in ethanol was also studied by FTIR transmission. A droplet of the Tb:SSA mixture diluted in ethanol was spread on a silicon wafer. The dried precipitate obtained after ethanol evaporation was studied in the (4000–300 cm^{-1}) spectral range. ORMOSIL films deposited on silicon wafers were studied by FTIR transmission in the (4000–300 cm^{-1}) range. FTIR spectrum of the bare silicon wafer used as substrate was recorded before film deposition and subsequently subtracted from the total (substrate + thin film) spectrum before analysis. The spectral resolution was 4 cm^{-1} both for ATR and transmission measurements. The thickness and refractive index of films deposited on silicon were measured using a Sentech ellipsometer operated at $\lambda = 632$ nm under 70° incidence. The film transparency was tested through UV/visible transmission spectrum measurements in the (200–1100 nm) range, by comparing the spectra of coated and uncoated silica plates. Spectra were collected using a JascoV-530 spectrophotometer. The spectral resolution was 1 nm. UV/vis transmission spectra were also used to determine the thickness value and the wavelength dependence of the refractive index for films deposited on silica, using a previously published procedure [26]. The refractive index at 632 nm was deduced from the dispersion curve using a Cauchy law. For photopolymerization experiments, films deposited on silicon or silica were thermalized at about 30°C and irradiated for 0 to 120 min using an UV lamp (UVP BLAK-RAY; 150 W/m^2) filtered at ca. 350 nm wavelength. PL spectra were measured in the 450–650 nm range by pumping at 355 nm in grazing incidence with a frequency tripled Nd:YAG pulsed laser (8 ns pulse duration; 10 Hz repetition rate) using a Jobin-Yvon H25 monochromator associated with a photomultiplier (Hamamatsu). PL was collected perpendicularly to the sample surface. For PL decay measurements, the photomultiplier was connected to a digital oscilloscope.

3. Results and discussion

3.1. Precursor solution characterization

The ATR-FTIR spectrum of a solution with a MTPS:TIPT molar ratio of 10:4 is presented in Fig. 1. Main IR features appeared in the (1800–850 cm^{-1}) spectral range [13, 27–30]. C═O stretching vibration of the α,β-unsaturated ester is depicted by a bi-component band with maxima at 1717 and 1703 cm^{-1}. The band at 1639 cm^{-1} corresponds to the C═C double bond of methacrylate groups. Other methacrylate components give rise to bands located at 1320, 1295, 1200, 1012, and 980 cm^{-1}. TIPT:MAA complex bands appear at 1550, 1508, 1423, and 1245 cm^{-1}. The band located at 1169 cm^{-1} is assigned to CH_3 rocking vibration from methoxy groups of MTPS. The band located at 950 cm^{-1} and the small shoulder around 920 cm^{-1} are assigned to Si─O^- stretching vibrations. Previous deconvolution studies have shown that the hydrolysis of alkoxy groups gives rise to a shift of the Si─O^- band towards lower wavenumber [31]. Thus, the band at 950 cm^{-1} is probably due to Si─OCH_3 bonds of the methoxy groups, while the 920 cm^{-1}shoulder would correspond to Si─OH bonds of hydrolyzed species. However, the 950 cm^{-1} band intensity was observed to significantly increase after TIPT:MAA complex incorporation in the solution, while the other methoxy

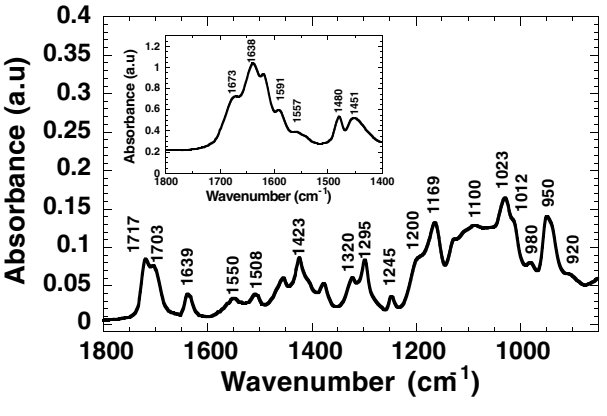

Figure 1 ATR-FTIR spectrum of a 10-4-8 MTPS-TIPT-MAA solution and (insert) FTIR spectrum of the complex formed from a Tb:SSA mixture.

band (1169 cm^{-1}) and the Si—OH band (920 cm^{-1}) decreased in intensity. IR absorption at 950 cm^{-1} is commonly attributed to Si—O—Ti mixed bonds [32]. Thus, the 950 cm^{-1} band depicted in Fig. 1 probably traduces the dual signature of methoxy groups and Si—O—Ti bonds. Si—O—Ti bonds would arise from a reaction between the TIPT:MAA complex and Si species. A band is observed at 1023 cm^{-1}, which appeared very intense after the first hydrolysis step ($r_w = 0.6$) and decreased in intensity after the TIPT:MAA complex incorporation. Besides, a large but weakly intense band appears around 1100 cm^{-1}, which was not observed before titanium complex incorporation. Asymmetric Si—O—Si stretching vibration bands are usually mentioned in this spectral region. It has also been reported that three-membered Si—O—Si cyclic species produce a band at 1023 cm^{-1} [33]. It is known that MTPS exhibits a weak sol-gel reactivity, which inhibits the formation of a silica network [34]. This is probably due to the steric hindrance of methacrylate groups that reduces the interaction probability between chain-end species. However, it is possible that a partial polycondensation reaction locally takes place between vicinal adjacent Si—OH species, which would promote the formation of Si—O—Si cyclic species. It has been reported that three-membered Si—O—Si cycles are strongly strained and can easily be opened to undergo new hydrolysis/polycondensation reactions giving rise to linear chains [35]. It is also known that the presence of titanium precursor activates the formation of Si—O—Si chains issued from hydrolysis/polycondensation of Si—OCH_3 and Si—OH species [36]. Thus, the broad band around 1100 cm^{-1} probably depicts the local development of Si—O—Si chains issued from further hydrolysis/polycondensation of Si—OCH_3, Si—OH, and cyclic species, which would be induced by the TIPT:MAA complex. Such a mechanism would explain the intensity decrease of bands at 1169, 1023, and 920 cm^{-1}, observed after titanium complex incorporation. To summarize, these data suggest that the titanium complex promoted a significant enhancement of the solution reactivity leading to the development of Si—O—Ti and Si—O—Si chains. After adding the complementary water amount to adjust r_w at 1.6, all the bands depicted in Fig. 1 appeared to be unchanged. This seems to indicate that main solution reactivity features were induced during the TIPT:MAA incorporation. However, it will be shown next that the final water addition plays a non-negligible role on the formation of homogeneous films.

The phase diagram of the Tb:SSA system (Fig. 2) has been derived from published stability constants for the different reaction products [37]. This diagram shows that precipitation of the terbium hydroxide can be prevented by a suitable adjustment of the pH and SSA concentration. Moreover, the formation of Tb:SSA complexed species appears to be very sensitive to acid-base conditions (insert of Fig. 2). In particular, Fig. 2 indicates that acidic conditions favor the formation of non-complexed free Tb^{3+} ions. Insert of Fig. 1 shows the FTIR spectrum of the Tb:SSA precipitate obtained

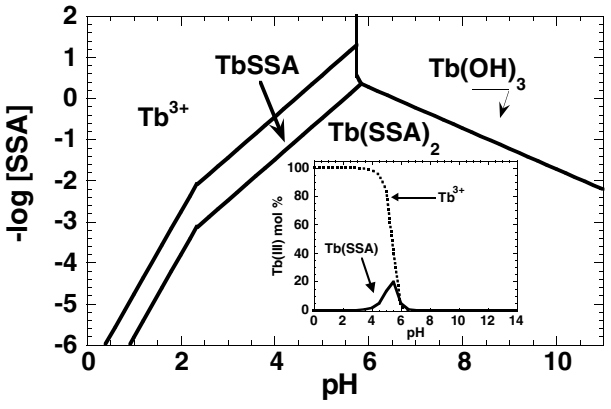

Figure 2 Tb:SSA binary phase diagram at 25°C (calculated for a Tb concentration of 5.8×10^{-2} M), and (insert) percent distribution of free Tb^{3+} and Tb:SSA complex (calculated for a SSA concentration of 5.8×10^{-2} M), as a function of pH. After the equilibrium constants reported by Martell and Smith [37].

after ethanol evaporation. Tb:SSA complexation was evidenced by three kinds of carboxylate binding sites giving rise to absorption bands at 1638, 1591, 1557, and 1451 cm^{-1} [27, 29]. Bands located at 1591 and 1557 cm^{-1} are assigned to asymmetric C—O stretching vibrations of the bridging and bidentate Tb-SSA complex, respectively. The C—O symmetric stretching vibration is observed at 1451 cm^{-1}. The band observed at 1638 cm^{-1} is related to the unidentate complex. Such features indicate that complexation of terbium with SSA takes place in natural ethanol pH conditions. However, the C═O vibration band of free SSA can also be observed at 1673 cm^{-1}, which indicates that SSA is not fully consumed by the complexation process. The 1480 cm^{-1} band corresponds to stretching vibration of C═C bonds, which are present both in free SSA and Tb:SSA complex. Due to the weak Tb concentration (11.6×10^{-2} M), FTIR spectroscopy did not allow to study the Tb:SSA complex once diluted in the MTPS solution. According to Fig. 2, it might be inferred that terbium undergoes partial de-complexation, owing to the rather acidic pH of the final solution (pH = 2 to 3). This aspect will be discussed in the next sections.

3.2. Film thickness and refractive index control

Fig. 3 shows the film thickness variations (measured after sol-gel transformation) versus deposition time and solution concentration for a 10MTPS-4TIPT-8MAA molar composition (we will next refer to 10-4-8 for simplification). The dashed line depicted in Fig. 3d ($C = 1.694$ M) indicates the short deposition time region where coalescence of droplets deposited on the substrate surface is incomplete, i.e., the number of deposited droplets is insufficient to ensure total coalescence. The resulting films appeared dotted and non-homogeneous. The continuous line in Fig. 3d indicates the region where homogeneous films (complete coalescence) can be produced. In that case, the thickness uniformity of the film after solvent evaporation and sol-gel reaction was determined to be about ±1%. For other

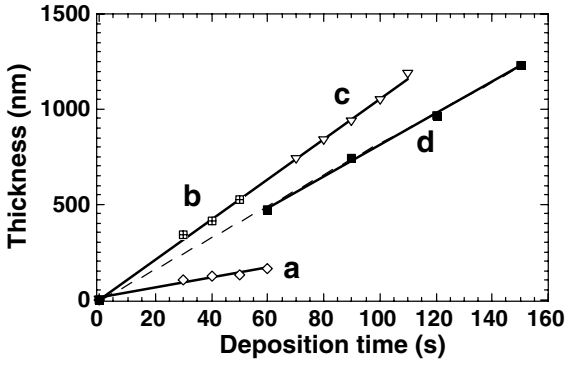

Figure 3 Film thickness versus deposition time for a 10MTPS-4TIPT-8MAA molar composition and various MTPS + TIPT concentrations (C): (a) $C = 0.154$ M, (b) $C = 0.658$ M, (c) $C = 1.428$ M, and (d) $C = 1.694$ M. The dashed line for $C = 1.694$ M indicates the region where droplet coalescence is incomplete (not shown for the other concentrations).

curves illustrated in Fig. 3, only experimental data corresponding to homogeneous films are presented (lines are drawn to guide the eyes). Fig. 3 shows that, for a given concentration, the film thickness increases linearly with the deposition time, which demonstrates that Aerosol-gel process allows a precise and flexible control of the deposition conditions for a film thickness up to 1.2 microns or more. In traditional Aerosol-gel deposition conditions, the deposition rate (R), i.e., the slope of straight lines illustrated in Fig. 3, is proportional to the flux of precursor [25]. In other words, for a constant aerosol production, R should linearly increase with the concentration (C) of precursor in the nebulized solution, i.e., the term $1/C \times R$ does not depend on the concentration. On the other hand, the aerosol production decreases for increasing solution viscosity. These features are illustrated in Fig. 4. It can be seen that the term $1/C \times R$ continuously decreases with increasing concentration. This was related to a viscosity increase from 2 to 3.5 cP for concentrations ranging from 0.154 to 1.904 M, which caused a decrease in the aerosol production yield. Films deposited from titanium-free solutions exhibited a poor optical quality. As mentioned above, pure MTPS sols have weak sol-gel reactivity, which inhibits gelation. For this reason, derived films generally undergo a liquid phase de-wetting mechanism related to surface tension of the liquid, which promotes orange-peel effects, thus preventing the deposition of optical quality films. In our conditions, orange-peel effects could efficiently be avoided when increasing the titanium precursor amount in the MTPS solution. This feature confirms FTIR data showing that the MTPS solution reactivity is activated in presence of titanium precursor, i.e., the titanium precursor promotes a fast post-deposition inorganic network development that counteracts the effects of surface tension and prevents liquid phase de-wetting. On the other hand, except for titanium-free solutions, the final water addition in the solution ($r_w = 1.6$) also played a favorable role in preventing de-wetting effects. This observation suggests that, despite the lack of changes depicted by FTIR spectra, additional water activates the sol-gel reaction taking place during the liquid-solid transformation of ORMOSIL films.

In the design of an integrated optical device, it is essential to have a precise knowledge of the refractive index. In particular, for integrated optical waveguides, the film refractive index has to be accurately adjusted with respect to the substrate refractive index and film thickness. The refractive index variations in bulk ORMOSIL gels have been described by the Claussius-Mosotti relationship [38]

$$(n^2 - 1)/(n^2 + 2) = 4\pi/3 \times \sum N_j \alpha_j$$

where n corresponds to the refractive index of the material, N_j to the concentration of the different components, and α_j to their electronic polarizability. In general the ionic polarizability increases with the ion size. As the ion size of Ti^{4+} (0.056 and 0.074 nm for tetrahedral and octahedral coordination, respectively) is larger than that of Si^{4+} (0.040 nm in tetrahedral coordination) [39], the film refractive index must continuously increase with the Ti^{4+} content. This is illustrated in Fig. 5, which shows variations of the Aerosol-gel film refractive index (632 nm) versus Ti concentration. The film thickness was 450 nm and the Ti:MAA molar ratio was 1:1. No post-deposition thermal treatment was performed. The refractive index continuously increases from 1.48 to 1.55 when increasing the Si:Ti ratio from 10:0 to 10:6, which shows that the film index can be flexibly controlled through a suitable Si:Ti

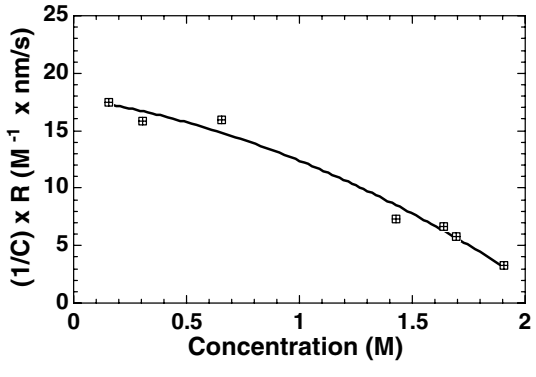

Figure 4 Normalized deposition rate ($1/C \times R$, where R is the slope of straight lines illustrated in Fig. 3) versus MTPS + TIPT concentration (C) for a 10-4-8 solution composition.

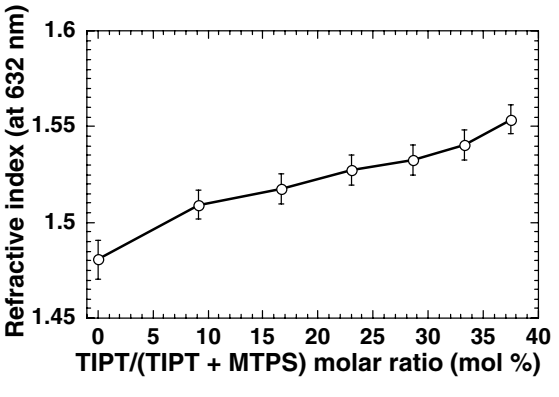

Figure 5 Refractive index versus TIPT/(TIPT + MTPS) molar concentration for Aerosol-gel deposited ORMOSIL films.

ratio adjustment. Similar variations were also observed for a Ti:MAA ratio of 1:2. Since the refractive index increase is not rigorously linear, it is not excluded as well that such an increase could also result from the catalytic effect of titanium species on sol-gel reaction, which would enhance the inorganic network development, thus influencing the ionic polarizability and refractive index. Refractive index values measured by ellipsometry and derived from UV/visible spectra for films deposited on silicon wafers and silica plates, respectively, appeared to be in good agreement. The refractive index of a 2.5 μm thick 10-4-8 film deposited on silica was measured to be 1.525 ± 0.006. A standard m-lines characterization showed that this film supported four TE/TM propagation planar modes at 632 nm. M-line characterization also confirmed the refractive index value derived from UV/visible spectra. A theoretical simulation indicated that a 0.7 μm thick film would be sufficient to propagate one single TE/TM mode. Such features suggest that Aerosol-gel deposited ORMOSIL films should be adapted for waveguiding applications.

3.3. FTIR characterization of ORMOSIL films

FTIR spectra of as-deposited 10-1-2 and 10-4-8 films are illustrated in Fig. 6a and b, respectively. For both films, the C═O methacrylate bond gives rise to a narrow single-band at 1719 cm^{-1}, which replaces the bi-component band evidenced for precursor solutions. The 1719 cm^{-1} wavenumber position agrees fairly well with published data for similar films [13]. All the other methacrylate bands described for MTPS-TIPT-MAA solutions (Fig. 1) remained unchanged after film deposition. Fig. 6a–b show that other bands identified in Fig. 1 are significantly modified by the titanium amount in the ORMOSIL matrix. TIPT:MAA complex bands are hardly detectable for the 10-1-2 film, while they clearly appear in the 10-4-8 film spectrum (see bands at 1245 and 1423 cm^{-1}). Bands observed around 940 and 920 cm^{-1} correspond to Si─OCH_3 and Si─OH species, respectively. For both films, the 940 cm^{-1} band is much less intense than that depicted in Fig. 1 for precursor solutions, which is attributed to the complementary hydrolysis/polycondensation of Si─OCH_3 species occuring during the liquid-solid film transformation. For the 10-4-8 film (Fig. 6b), a small shoulder is observed to grow at 950 cm^{-1}, on the high wavenumber side of the methoxy band, which is hardly detectable for the 10-1-2 film (Fig. 6a). This shoulder illustrates the development of Si─O─Ti bonds when increasing the titanium amount in the ORMOSIL matrix. In Fig. 6a–b, the Si─O─Si cycle band (1023 cm^{-1}) depicted for precursor solutions has nearly vanished. Besides, the broad band assigned to Si─O─Si chains has strongly increased in intensity, which confirms that polycondensation occurred to a large extent during the solid-liquid transformation, giving rise to the consumption of Si─O─Si cycles and methoxy groups. In Fig. 6a, the Si─O─Si band is centered around 1125 cm^{-1}. The remarkably high wavenumber position of this band is a common feature in MTPS-derived ORMOSIL films [13], which probably depicts Si─O─Si chains linked to methacrylate groups. For the 10-4-8 film, the Si─O─Si band broadens towards lower wavenumbers, leading to a broad band centered around 1110 cm^{-1}. As will be shown below, this broadening is presumably due to the development of silica chains that would be activated by a greater titanium amount in the ORMOSIL matrix.

It is known that UV-light irradiation triggers the polymerization of the acrylate function. However, polymerization or decomposition of the acrylate function can be thermally induced as well. In either case, optical properties of the film are modified. When studying a photopolymerizable system, it is therefore important to check that the process is actually induced by a photochemical event and not by a thermal reaction. The effects of thermal treatment were thus subjected to a preliminary study by FTIR spectroscopy. Spectra of 10-4-8 films heat-treated for 2 h at various temperatures are presented in Fig. 6c–f. C═C (1639 cm^{-1}) and C═O (1719 cm^{-1}) bonds appear to be noticeably modified by heat-treatment. The thermally induced conversion rate (R_C) of C═C bonds has been deduced from the 1639 cm^{-1}band area (A) using the relationship

$$R_C = (A_0 - A)/A_0$$

where A_0 corresponds to the band area before heat-treatment. The conversion rate variations versus heat-treatment temperature are illustrated in Fig. 7. It can

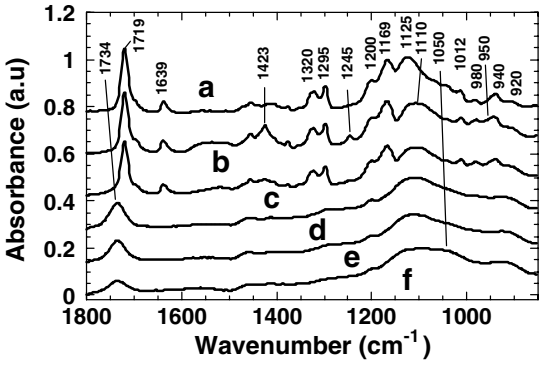

Figure 6 FTIR characterization of (a) 10-1-2 and (b) 10-4-8 films before heat-treatment, and 10-4-8 films after heat-treatment for 2 h at (c) 100°C, (d) 150°C, (e) 200°C, and (f) 250°C.

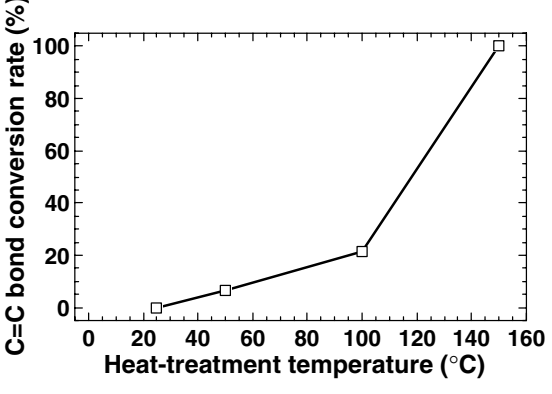

Figure 7 Conversion rate of the C═C double bond versus heating temperature for a 10-4-8 film. Data are derived from FTIR spectra of Fig. 6.

be seen that the C═C conversion rate continuously increases with increasing temperature up to 150°C. Conversion seems to be completed at this temperature. In the same time, Fig. 6 shows that the C═O stretching band broadens and shifts from 1719 cm^{-1} towards 1734 cm^{-1}, but varies very weakly in intensity (area of the C═O band). These changes are accompanied with the disappearance of main methacrylate bands (1320, 1295, 1200, 1012 and 980 cm^{-1}). Then, the C═O band does not vary anymore in position, but it is observed to continuously decrease in intensity when increasing temperature from 150 to 250°C. This feature probably indicates that methacrylate species are decomposed above 150°C. Fig. 6a–c also show that main bands related to TIPT:MAA complex (1423 and 1245 cm^{-1}) and methoxy groups (940 and 1169 cm^{-1}) decrease in intensity with increasing temperature from 25 to 150°C and nearly vanish after heat-treatment at 150°C, which indicates the consumption of both kinds of species. Finally, the 1110 cm^{-1} band also decreases in intensity with increasing temperature and broadens towards lower wavenumbers, giving rise to a large shoulder around 1050 cm^{-1}. This wavenumber position corresponds to asymmetric stretching vibration (TO_3 mode) of Si─O─Si chains in a pure silica network. This feature confirms that the Si─O─Si broadening observed in Fig. 6b is due to the development of Si─O─Si chains induced by the presence of a greater amount of titanium. Besides, variations of the methoxy and Si─O─Si bands illustrated in Fig. 6c–f clearly depict a thermally activated hydrolysis/polycondensation mechanism. To summarize, Ti and Si bands variations suggest that thermally induced C═C and C═O bond changes are accompanied with modifications of the inorganic network, i.e., thermally induced TIPT:MAA complex decomposition and Si─O─Si chain development. On the other hand, Fig. 7 clearly shows that, in our UV-irradiation conditions (thermalization at 30°C; irradiation for 0 to 120 min), thermally induced effects can be neglected.

3.4. Photopolymerization and photo-densification features

Fig. 8 shows the effect of UV-irradiation on the FTIR spectra of 10-4-8 films doped or not with BZK photoinitiator. Spectra illustrated in Fig. 8 show a progressive intensity decrease of the C═C band with increasing

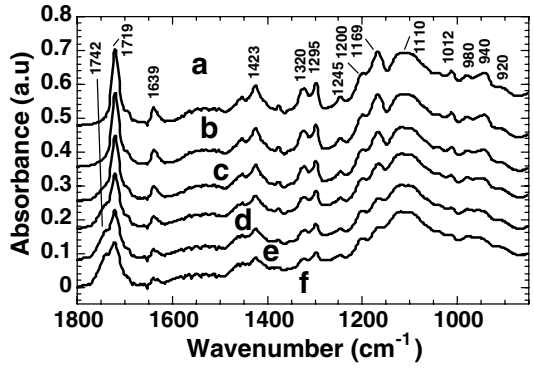

Figure 8 FTIR spectra of 10-4-8 films exposed to UV-irradiation for (a) 0 min, (b) 10 min, (c) 30 min, (d) 60 min, (e) 90 min, and (f) 120 min.

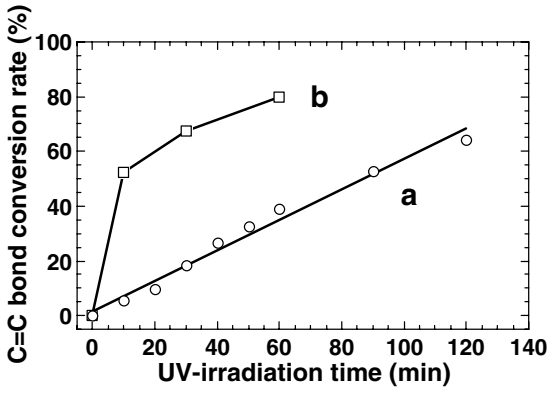

Figure 9 Conversion rates of the C═C double bond for (a) undoped and (b) BZK-doped 10-4-8 films exposed to UV-irradiation. Data are derived from FTIR spectra of Fig. 8.

irradiation time, which indicates that photopolymerization of the methacrylate groups continuously takes place. The C═C double bond conversion rate is illustrated in Fig. 9 for BZK-doped and non-doped films of 1.2 μm in thickness. Conversion is much faster for the doped film. The conversion rate rapidly increases up to 50% after 10 min UV-irradiation and then increases more slowly, reaching a value of 80% after 60 min UV-irradiation. For the non-doped film, the conversion rate increases nearly linearly, reaching a value around 60% after 120 min UV-irradiation. Besides, the C═O stretching band at 1719 $cm^{-1}$is observed to decrease in intensity during the photopolymerization process and to be progressively replaced by a new band located at 1742 cm^{-1}. Such features presumably depict changes induced by polymerization in the C═O bond environment [14]. After 120 min UV-irradiation (Fig. 8f), the bi-component C═O band forms a broad band centered around 1734 cm^{-1}. Fig. 8 also indicates that, during UV-polymerization, bands related to TIPT:MAA complex (1423 and 1245 cm^{-1}) and methoxy groups (940 and 1169 cm^{-1}) undergo the same variations as for thermal treatment, i.e., the photo-induced polymerization of methacrylate groups is accompanied with partial TIPT:MAA complex decomposition and Si─O─Si chain development.

UV-irradiation was also observed to significantly modify the refractive index and thickness of the films. Fig. 10 shows the visible transmittance spectra of a

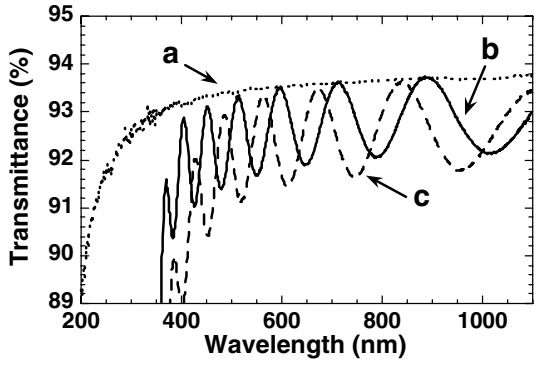

Figure 10 Visible transmittance spectra of (a) a bare silica plate, (b) a silica plate coated with a 10-4-8 ORMOSIL film, and (c) the same sample after 60 min UV-irradiation.

10-4-8 BZK-doped film deposited on a silica plate, before UV-irradiation and after irradiation for 60 min. For both films, the strong edge absorption observed below 400 nm is presumably due to the TiO_2 component of the film. Both spectra exhibit interference fringes related to multi-reflections at the film-air and film-substrate interfaces. For a transparent film of high refractive index ($n \approx 1.52$ for the non-irradiated film) deposited on a transparent substrate of lower refractive index ($n = 1.45$ for silica), transmission maxima are obtained when the film optical thickness corresponds to even multiples of the quarter-wavelength. At these wavelengths, the film is theoretically optically non-active, i.e., for an optical quality film, the transmission values should fit the bare substrate transmission. Transmission minima are obtained when the film optical thickness corresponds to odd multiples of the quarter-wavelength, i.e., when the mismatch of refractive indices between substrate and film induces a maximum of reflection. The intensity of interference fringes is therefore expected to increase with increasing refractive index. For both spectra shown in Fig. 10, transmittance maxima fit fairly well the bare silica substrate transmittance (above 500 nm, the discrepancy is smaller than 0.5% in transmittance, i.e., the experimental accuracy), which indicates the good transparency of the film, i.e., negligible absorption or scattering losses. From Fig. 10, it can thus be concluded that UV-irradiation did not cause any degradation of the film optical quality. On the other hand, significant modifications of the interference fringe position and intensity can be observed after irradiation, i.e., the fringes are more pronounced, which depicts a greater refractive index, and the transmission extrema are shifted toward shorter wavelengths, which depicts a thickness decrease. Such variations indicate that UV-irradiation induces film densification. Film thickness and refractive index values were deduced from the envelopes of the transmission maxima and minima, using a formalism proposed by Swanepoel (see ref. [26] for details). Fig. 11 shows that, in the presence of BZK photoinitiator, refractive index and thickness variations are closely related to the C=C double bond conversion rate (see Fig. 9b), which indicates that densification arises from photo-induced transformations of the mixed organic/inorganic network depicted in Figs 8 and 9. Fig. 11 shows that, after 60 min irradiation, the refractive index increase is about 0.012, while the thickness decreases by about 6%. The refractive index increase is comparable to previously published data for similar films [10, 13]. Such features demonstrate the feasibility of UV-writing Aerosol-gel deposited ORMOSIL films. Similar photo-induced densification effects were also observed for BZK-free films (not shown here), but the refractive index and thickness variations were much weaker than those measured for BZK-doped films, which is in agreement with the smaller conversion rate depicted in Fig. 9a. Let us note that photo-induced densification features illustrated in Fig. 11 correspond to non-cured films. Densification features appeared to be less important when the films were heat-treated at low temperature before UV-irradiation, and no photo-induced effects could be evidenced for films subjected to preliminary heat-treatment at 150°C or more. As shown in Figs 6 and 7, this was due to the thermally induced C=C bond conversion, which promoted a loss of the film photosensitivity.

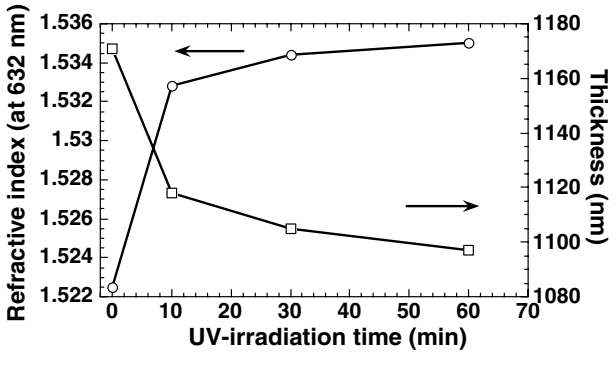

Figure 11 Refractive index and thickness variations for a 10-4-8 BZK-doped film exposed to UV-irradiation for various times.

3.5. PL properties

Fig. 12 shows the PL spectrum in the (450–650 nm) range of a Tb:SSA doped ORMOSIL film heat-treated at 150°C. The spectrum exhibits characteristic emission lines of Tb^{3+} ions, i.e., the $^5D_4 \rightarrow {}^7F_J$ ($J = 6, 5, 4, 3$) transitions centered at 490, 545, 585, and 620 nm, respectively. The typical green emission of Tb^{3+} ions corresponding to the $^5D_4 \rightarrow {}^7F_5$ transition appears to be dominant. The peak observed at 532 nm corresponds to the second harmonic generation of the Nd:YAG laser pump emission. Measurements of the PL intensity at 545 nm, normalized with respect to the pump intensity (peak at 532 nm), show that the heat-treatment temperature significantly influences the spectroscopic performances of the films (insert of Fig. 12). The PL intensity increases when increasing the temperature in the (25–150°C) range. It increases slowly in the (25–100°C) range and suddenly jumps when increasing the temperature from 100 to 150°C. The PL intensity is then observed to continuously decrease when increasing again the temperature. These features can be discussed in terms of hydroxyl content (mainly Si–OH species) in

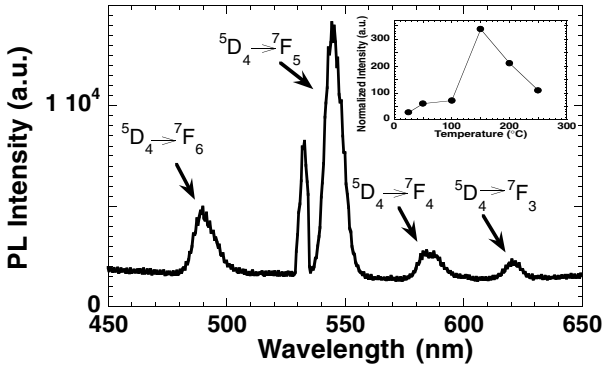

Figure 12 PL spectrum (355 nm pumping) of a 10-4-8 ORMOSIL film doped with 1:0.5 Tb:SSA complex and heat-treated for 2 h at 150°C, and variations of the normalized PL intensity (545 nm) versus heat-treatment temperature (insert). The peak at 532 nm, which is related to the laser pump, has been used as reference to normalize the PL intensity of the films.

the films and encapsulation efficiency of the SSA cage. As shown in Fig. 1, SSA was not fully consumed by terbium complexation. It can thus be presumed that the encapsulation efficiency is not optimal, so that PL quenching effects induced by hydroxyl groups remain predominant after heat-treatment at low temperature. Fig. 6 showed that the polycondensation reaction was thermally activated, which progressively reduced the hydroxyl content in the film when the heating temperature was increased. Thus, despite the unavoidable presence of residual hydroxyl groups, the organic encapsulation efficiency becomes sufficient to prevent PL quenching effects. This leads to a noticeable increase of the PL intensity after heating at 150°C. On the other hand, it has been reported that the Tb:SSA complex undergoes progressive thermal dissociation, as soon as the temperature exceeds 150°C [17]. The same observation was made on Aerosol-gel deposited SiO_2–TiO_2 films doped with Tb:SSA complex [22]. Therefore, a temperature increase above 150°C reduces the encapsulation efficiency and terbium ions are again exposed to interactions with hydroxyl groups. This yields a progressive decrease of the PL intensity. It is also possible that decomposition of the methacrylate network, depicted in Fig. 6 for temperatures greater than 150°C, induces the production of new OH species. This would also contribute to quench the PL. The PL intensity was not modified when the films were preliminarily photopolymerized before heat-treatment. On the other hand, no photopolymerization features could be evidenced after heat-treatment at 150°C. These observations imply that the UV-imprinting fabrication of optically active integrated devices should involve first the photopolymerization of as-deposited films, followed by heat-treatment to optimize the PL properties.

Fig. 13 shows the PL decay curve at 545 nm for a film heat-treated at 150°C. The film exhibits a bi-exponential decay, which is composed of a fast decay component with a first e-fold lifetime of only 22 μs, and a slow component with a lifetime of 230 μs. The slow component lifetime agrees fairly well with values previously measured on bulk silica gels doped with terbium:SSA complex [22]. The bi-exponential PL decay could be explained by two kinds of terbium environments in the host matrix. In a first environment where encapsulation in the SSA cage is insufficient, the terbium ions would be exposed to interactions with hydroxyl groups, which would promote PL quenching effects leading to the very short lifetime. In a second environment, efficient encapsulation would shield terbium ions against interactions with hydroxyl groups, which would produce the slow PL decay component. Thus, it is possible that partial decomposition of the Tb:SSA complex and/or additional hydroxyl group production start to take place during heat-treatment at 150°C. As indicated in Fig. 2, it could also be possible that terbium undergoes partial decomplexation once mixed in the acidic MTPS solution. However, we previously showed that bulk silica gels, prepared from acidic solution (pH of 2) and doped with Tb:SSA complex, exhibited a single exponential decay. This observation implies that acidic conditions used for our solution preparation do not affect significantly the PL properties of ORMOSIL films, i.e., the Tb:SSA complex should not undergo decomplexation induced by the acidic MTPS solution. Further experiments are now in progress to better understand and to optimize the terbium ion behaviors in photocurable ORMOSIL films.

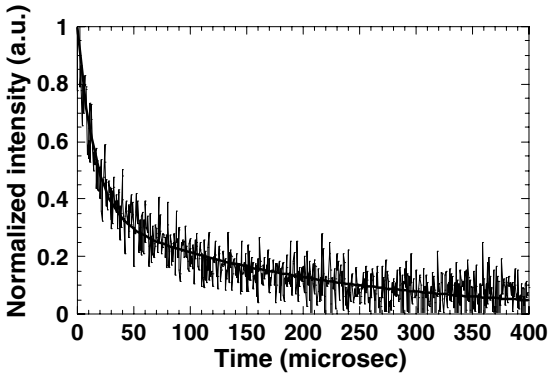

Figure 13 PL decay curve (PL emission at 545 nm) of a 10-4-8 film doped with Tb:SSA complex and heat-treated at 150°C for 2 h. The PL decay is fitted with a bi-exponential curve. The first e-fold lifetime is deduced to be 22 μs. The slow decay component lifetime is deduced to be 230 μs.

4. Conclusion

Photocurable and optically active SiO_2–TiO_2 ORMOSIL films containing methacrylate groups and doped with terbium complex were deposited using the Aerosol-gel process. The films exhibit a good optical quality. UV-irradiation experiments show that photopolymerization of the methacrylate groups favors complementary polycondensation of the inorganic network. This is accompanied with the densification of the ORMOSIL matrix, which leads to a significant refractive index (thickness) increase (decrease). Thus, Aerosol-gel deposited ORMOSIL films appear to be adapted to the UV-impriting fabrication of channel waveguides. Photopolymerization effects under UV-irradiation have been observed both in BZK-doped and non-doped films. However, the C=C double bond conversion appears to be less effective in the absence of BZK photoinitator. Besides, the organic encapsulation of terbium ions within an organic SSA cage yields good PL properties in thin films heat-treated at low temperature. Optimal PL intensities have been measured on films heat-treated at 150°C. Thus, this work is a promising first step toward the UV-imprinting fabrication of Aerosol-gel-derived active waveguides for applications in integrated optics.

References

1. H. SCHMIDT, A. KAISER, H. PATZELT and H. SHOLZE, *J. Phys.* **12**(43) (1982) 275.
2. D. AVNIR, D. LEVY and R. REISFELD, *J. Phys. Chem.* **88** (1984) 5956.
3. D. A. LOY, *MRS Bull.* **26**(5) (2001) 364.
4. C. SANCHEZ and B. LEBEAU, *ibid.* **26**(5) (2001) 377.
5. H. KRUG and H. SCHMIDT, *New J. Chem.* **18**(10) (1994) 1125.
6. B. DUNN, J. D. MACKENZIE, J. I. ZINK and O. M. STAFSUDD, *SPIE Proc.* **1328** (1990) 174.
7. H. SCHMIDT, H. KRUG, R. KASEMANN and F. TIEFENSEE, *ibid.* **1590** (1991) 36.

8. P. COUDRAY, J. CHISHAM, A. MALEK-TABRIZI, C. Y. LI, M. P. ANDREWS, N. PEYGHAMBARIAN and S. I. NAJAFI, *Opt. Comm.* **128** (1996) 19.
9. D. L. OU, A. ADAMJEE, S. L. LANA and A. B. SEDDON, *Surf. Coat. Int.* **11** (1996) 496.
10. P. COUDRAY, J. CHISHAM, M. P. ANDREWS and S. I. NAJAFI, *Opt. Eng.* **36**(4) (1997) 1234.
11. P. ETIENNE, P. COUDRAY, Y. MOREAU and J. PORQUE, *J. Sol-Gel Sci. Tech.* **13** (1998) 523.
12. P. INNOCENZIE, A. MARTUCCI, M. GUGLIELMI, L. ARMELAO, S. PELLI, G. C. RIGHINI and G. C. BATTAGLIN, *J. Non-Cryst. Sol.* **259** (1999) 182.
13. O. H. PARK, J. I. JUNG and B. S. BAE, *J. Mater. Res.* **16**(17) (2001) 2143.
14. O. SOPPERA, C. CROUTXE-BARGHORN and D. J. LOUGNOT, *New J. Chem.* **25** (2001) 1006.
15. L. SLOOF, A. POLMAN, M. OUDE WOLBERS, F. VAN VEGGEL, D. REINHOUDT and J. HOFSTRAAT, *J. Appl. Phys.* **83** (1998) 497.
16. V. BEKIARI, P. LIANOS and P. JUDENSTEIN, *Chem. Phys. Lett.* **307** (1997) 310.
17. X. FAN, M. WANG, Z. WANG and Z. HONG, *Mater. R. Bull.* **32** (1997) 1119.
18. M. LANGLET and J. C. JOUBERT, European Patent no. 0486393 (1991).
19. Brite-Euram Project 7765, Contract no. BRE2-CT94-0985 (1994–1998).
20. C. COUTIER, M. AUDIER, J. FICK, R. RIMET and M. LANGLET, *Thin Solid Films* **372** (2000) 177.
21. C. COUTIER, W. MEFFRE, P. JENOUVRIER, J. FICK, M. AUDIER, R. RIMET, B. JACQUIER and M. LANGLET, *ibid.* **392** (2001) 40.
22. P. JENOUVRIER, E. CELA, C. COUTIER, M. LANGLET, R. RIMET and J. FICK, *Appl. Phys.* B **73** (2001) 1.
23. M. LANGLET, C. COUTIER, J. FICK, M. AUDIER, W. MEFFRE, B. JACQUIER and R. RIMET, *Opt. Mater.* **16** (2001) 463.
24. M. LANGLET, P. JENOUVRIER, J. FICK and R. RIMET, *J. Sol-Gel Sci. Tech.* **26** (2003) 985.
25. M. LANGLET, C. VAUTEY and N. MAZEAS, *Thin Solid Films* **299** (1997) 25.
26. R. SWANEPOEL, *J. Phys. E: Sci. Instrum.* **16** (1983) 1214.
27. G. SOCRATES, "Infrared Characteristic Group Frequencies" (John Wiley & Sons, 1994).
28. L. J. BELLAMY, "The Infra-Red Spectra of Complex Molecules" (Chapman and Hall, London; Wiley, 1975) p. 183.
29. K. NAKAMOTO and P. J. McCARTHY, "Spectroscopy and Structure of Metal Chelate Compounds" (S. J. John Wiley & Sons, 1968) p. 216.
30. W. J. E BECK and R. A. J. JANSEN, *Adv. Funct. Mater.* **12** (2002) 519.
31. N. PRIMEAU, C. VAUTEY and M. LANGLET, *Thin Solid Films* **310** (1997) 47.
32. C. U. INGEMAR ODENBRAND, S. LARS T. ANDERSSON, LARS A. H. ANDERSSON, JAN G. M. BRANDIN and G. BUSCA, *J. Catal.* **125** (1990) 541.
33. C. A. CAPOZZI, L. D. PYE and R. A. CONDRATE S., *Mater. Lett.* **15** (1992) 130.
34. C. A. CAPOZZI and L. D. PYE, *SPIE Proc.* **970** (1988) 135.
35. S. WALLACE, J. K. WEST and L. L. HENCH, *J. Non-Cryst. Sol.* **152** (1993) 101.
36. C. J. BRINKER and G. W. SCHERER, "Sol-Gel Science, The Physics and Chemistry of Sol-Gel Processing" (Academic Press, San Diego, 1990) p. 226.
37. A. E. MARTELL and R. M. SMITH, "Critical Stability Constants 3" (Other Organic Ligands, 1977) p. 190.
38. E. J. A. POPE, M. ASAMI and J. D. MACKENZIE, *J. Mater. Res.* **4** (1989) 1018.
39. J. E. HUHEEY, "Inorganic Chemistry," 3rd ed. (Harper & Row Publishers, New York, 1983) p. 75.

Received 10 February
and accepted 17 December 2003